Journal of Inorganic and General Chemistry
ZAAC
Zeitschrift für anorganische und allgemeine Chemie
DOI: 10.1002/zaac.202000360
ARTICLE

Structure and properties of fluorinated and non-fluorinated Ba-coordination polymers – the position of fluorine makes the difference

Steffen Zänker,[a, b] Gudrun Scholz,*[a] Wenlei Xu,[a] Franziska Emmerling,*[a, b] and Erhard Kemnitz[a]

As the most electronegative element, fluorine has a strong influence on material properties such as absorption behaviour or chemical and thermal stability. Fluorine can be easily integrated into coordination polymers (CPs) via a fluorinated acetate, here trifluoroacetate in $Ba(CF_3COO)_2$, or directly via a metal fluorine bond ($BaF(CH_3COO)$). In the present study both possibilities of fluorine integration were tested and their effect on structure and properties of barium coordination polymers was investigated in comparison with the non-fluorinated barium acetate ($Ba(CH_3COO)_2$). In addition to the study of their thermal behaviour and their decomposition temperature, the CPs structures were tested for their application as possible anode materials in lithium ion batteries and for their sorption of water and ammonia. The properties of the CPs can be traced back to the individual structural motifs and could thus trigger new design ideas for CPs in LIBs and/or catalysis.

Introduction

Coordination polymers (CPs) are well suited for different applications because of the easy tunability of these LEGO like structures.[1] Changes in both linker and metal allow the properties of CPS to be tuned and they are likely to play a key role in energy system transformation.[2] CPs are already used for sensors,[3] adsorption chillers,[4] catalysis,[5] hydrogen storage,[6] adsorption heat pumps,[7–10] and lithium-ion batteries (LIB).[11,12] CPs with particularly large surface are considered as attractive materials for hydrogen storage. A critical issue in hydrogen storage is that the hydrogen molecule has no dipole moment and is very difficult to polarize.[13] Hydrogen molecules can be attached to the surface of the CPs by physisorption. To bind hydrogen on the surface by polarization effects, halogenated linkers are used.[14] Fluorine plays a key role in this process. CPs with fluorinated linkers have a significantly increased hydrogen storage capacities.[15–17] Fluorinated CPs are also of interest for the development of new anode materials for lithium ion batteries (LIB). Here, the high electronegativity of fluorine is crucial for interactions with Li^+ ions and anode materials.[18] The fluorination of anode surfaces is another possibility to integrate fluorine into LIBs.[19,20] An improvement of the Li^+ transfer on the active material is always observed, if fluorine is used as a dopant, and this is attributed to the formation of defects in the structure. These defects facilitate diffusion in the anode material and allow easier access to the metal centres.[21–23] In addition, the metal fluorine bond protects the material against the attack of HF, which is formed during the hydrolysis of the electrolyte lithium hexafluorophosphate, $LiPF_6$.[24]

Several CPs with fluorinated linkers can be found in the literature whereas only a few examples of CPs with a direct metal-fluorine bond have been reported.[25–36] The first compounds with this structural element belong to the MF(*p*-BDC) family (M: metal atom, *p*-BDC: 1,4-benzenedicarboxylic). The metals are octahedrally coordinated by oxygen and fluorine. The octahedrons are connected by fluorine to form chains. The chains build a three dimensional network with the 1,4-benzenedicarboxylic acid.[37] Another representative of this family is the compound AlF(*p*-BDC).[38] This compound is isostructural to AlOH(*p*-BDC).[39] Unlike AlOH(*p*-BDC), AlF(*p*-BDC) does not absorb water at ambient temperature. Water absorption in AlOH(*p*-BDC) occurs preferentially at the free hydroxide group, whereby the possible formation of hydrogen bonds is investigated. A similar behaviour can be observed for Ga(OH,F)(*p*-BDC)[40] with a mixed OH^-/F^- coordination. Ga-(OH,F)(*p*-BDC) absorbs less water than the non-fluorinated network due to the hydrophobic character of fluorine. In this structure, only a small part of the hydroxide groups has been exchanged by fluorine and therefore the hydrophobic character of the metal centre is not as pronounced as in the AlF(*p*-BDC). CPs with structural elements that prevent water retention on the metal ion should be significantly less sensitive to hydrolysis starting with a nucleophilic attack of water molecules on the

[a] *M.Sc. S. Zänker, PD Dr. G. Scholz, M.Sc. W. Xu, PD Dr. F. Emmerling, Prof. Dr. E. Kemnitz*
Humboldt-Universität zu Berlin, Department of Chemistry, Brook-Taylor-Str. 2, D-12489 Berlin, Germany
E-mail: Gudrun.Scholz@rz.hu-berlin.de
franziska.emmerling@bam.de
[b] *M.Sc. S. Zänker, PD Dr. F. Emmerling*
Federal Institute for Materials Research and Testing (BAM), Richard-Willstätter-Str. 11, D-12489 Berlin Germany

Supporting information for this article is available on the WWW under https://doi.org/10.1002/zaac.202000360

© 2021 The Authors. Zeitschrift für anorganische und allgemeine Chemie published by Wiley-VCH GmbH. This is an open access article under the terms of the Creative Commons Attribution License, which permits use, distribution and reproduction in any medium, provided the original work is properly cited.

metal ion.[41,42] The metal ion-linker bond is the structure's weakest point.[43] A strong metal ion-linker bond is formed when the polarizabilities of the metal and the linker are almost similar.[44] Not only the structural motif of a direct metal ion - fluoride bond has an influence on the interaction with water, but also the various fluorine positions at the linker influence the vapour absorption behaviour.[45–47] The absorption and desorption process of water on the CPs is important for the design of thermally driven adsorption chillers (TDC) or adsorption heat pumps (AHP).[7] Basic requirement of such plants are water stable CPs.

To date, there are no comparative studies between coordination polymers with perfluorinated linkers and coordination polymers with a direct metal ion-fluoride bond. For a comparison, the selected CPs should be composed of linkers with the same carbon skeleton, metal, and a similar chemical composition but consider the two different fluorine positions in the networks.

Here we compare structure and properties of three different Ba-coordination polymers differing by the fluorine position in the network. The CPs structures are tested for their potential application as anode materials in lithium ion batteries and for their sorption of water and ammonia. The following CPs were selected for the comparison: barium acetate fluoride BaF(CH_3COO) with a direct metal-fluorine bond, barium trifluoroacetate $Ba(CF_3COO)_2$ with a perfluorinated linker, and the non-fluorinated barium acetate $Ba(CH_3COO)_2$. The position of fluorine has a strong influence on material properties such as absorption behaviour or chemical and thermal stability of CPs and their performance as anode materials in LIBs.

Experimental Part

Synthesis

All starting materials were used as commercially purchased (Table SI-1). Barium acetate was purchased from Sigma Aldrich (Purity $\geq$ 99 %). BaF(CH_3COO)$_2$ was synthesized from barium acetate and HF dissolved in ethanol. Barium acetate was dissolved in a mixture of 1 part acetic acid (Fluka, (Purity $\geq$ 98 %)), 3 parts ethanol ((Fluka, (Purity $\geq$ 98 %) (v:v)), and a stoichiometric amount of HF (Nanofluor GmbH, Purity $\geq$ 95 %) was added to the mixture. After two days the solvent was removed and the resulting powder was dried under vacuum at 150 °C.[48] To prepare $Ba(CF_3COO)_2$, 1 g barium carbonate was dissolved in 20 mL trifluoroacetic acid.[49] After gas evolution stopped, the solvent was removed under reduced pressure.

Thermal analysis

The thermal behaviour was studied with a NETZSCH thermoanalyzer STA 409C Skimmer, additionally equipped with a conventional high temperature SiC oven. A DTA-TG sample carrier system with platinum crucibles (baker, 0.8 mL) and Pt/PtRh10 thermocouples were used. Measurements were performed in a nitrogen atmosphere applying a heating rate of 10 K min^{-1}.

Brunauer-Emmett-Teller (BET) measurements

BET gas adsorption experiments were carried out on an ASAP 2010 (Micromeritics) using a 1 Torr pressure transducer with a resolution of 5–10^{-5} Torr (0.007 Pa). The adsorptive used was nitrogen at a temperature of 77 K. Prior to the measurements, samples were degassed at room temperature for 24 h under vacuum (10 Pa).

Dynamic vapour sorption (DVS)

Dynamic vapour sorption (DVS) experiments were performed on the DVS-1 instrument (Surface Measurements Systems, London, UK). The DVS system is a gravimetric sorption apparatus which consists of a sample chamber with a thermostat for maintaining a constant temperature of the sample and a flow controller for producing a controllable variable vapour pressure. The adsorbed mass was determined by continuous weighing as a function of the relative pressure. The sensitivity of the DVS-1 system is 0.1 μg and the dynamic range 150 mg. The accuracy of the system is $\pm$1 % for the relative humidity (RH) over a range of 0–98 %. A rate of change in mass per time unit (dm/dt) of 0.001 % min^{-1} was set as the equilibration parameter. Water was used for the dehydrated samples to study the phase transitions of hydrated/dehydrated samples.

Temperature-programmed desorption of ammonia (NH_3—TPD)

In a quartz flow reactor 0.2 g of coordination polymers were added and heated at 100 °C under nitrogen flow for 1 hour. Ammonia was adsorbed on the surface after cooling down until 80 °C. The desorption was performed using a heating rate of 10 °C min^{-1} up to 500 °C and kept at 500 °C at 40 min. The process was monitored by FT-IR spectroscopy (FT-IR System, PerkinElmer) by following the Intensity of band at 930 cm^{-1}. The total amount of ammonia desorbed was quantified by back-titration with a sodium hydroxide solution after treatment with excess sulfuric acid.

Cell assembling and electrochemical test

For the working electrodes, a slurry was prepared by mixing Ba-coordination polymers, carbon black (Super C65, Timcal) conductive additive and PVDF binder (Alfa Aesar) in N-methyl-2-pyrrolidine (NMP, Sigma-Aldrich, 99.5 %) with a mass ratio of 6:2:2. The slurry was cast onto a copper foil (25 μm, Goodfellow) with a doctor blade apparatus and the coated films were subsequently dried at 70 °C. After a cold-laminating step, electrodes with a diameter of 18 mm were punched out and dried overnight at 120 °C under vacuum using a Büchi glass oven. Coin cells type CR2032 were used for the batteries that were fabricated in a Ar-filled glovebox. The electrolyte was a 1 M $LiPF_6$ (ABCR, 99.9 % battery grade) solution in a mix of ethylene carbonate (ABCR, 99.9 %), propylene carbonate (ABCR, 99.9 %), and dimethyl carbonate (ABCR, 99.9 %) (1:1:1 by volume). A lithium foil was used as counter/reference electrode and a glass microfiber filter (Whatman) was used as separator. Tests of galvanostatic charge and discharge were performed between 0.5 and 3.0 V (vs Li/Li$^+$) with a CT2001 A cell test instrument (LAND Electronic Co.). Cyclic voltammetry was carried out using a Bio-Logic VMP3 multichannel potentiostat/galvanostat.

© 2021 The Authors. Zeitschrift für anorganische und allgemeine Chemie published by Wiley-VCH GmbH

Results and Discussion

The selected CPs differ in the fluorine positions in the network. In barium trifluoroacetate $Ba(CF_3COO)_2$ structure fluorine is integrated in the network via the linker, whereas fluoride is directly bound to the metal in the $BaF(CH_3COO)$ structure. In the few fluorinated coordination polymers known, in which fluorine is directly bound to the metal, fluorine usually bridges the metal centers with each other. Barium acetate fluoride[48] crystallizes in a 2D layered structure. The coordination number of barium in $BaF(CH_3COO)$ is six (Figure 1c with the local coordination $[BaF_2O_4]$). This untypical low coordination number for Ba is surprising since fluorine only requires a small amount of space. The coordination polyhedra of fluoride and barium ions bridges the units along the *a* and *c* axes. The acetate groups separate the layers. Through van der Waals interactions, layers are held together. The distance between the layers is 2.96 Å. There are only few known exceptions in the literature where fluorine is terminally bound to the metal directed into channels or pores instead of connecting the coordination polyhedra. One would expect that the most electronegative element is surrounded by cations.

In barium trifluoroacetate ($Ba(CF_3COO)_2$[50] the fluorinated methyl groups point into the channels (Figure 1b). The channels have an average diameter of 3.45 Å. The metal ions are only linked by the oxygen atoms of the carboxylic groups. The coordination number of eight is higher than in the analogous network with a direct metal ion - fluoride bond. When comparing the networks formed by perfluorinated linkers with those of non-fluorinated linkers, it is obvious that the structures are similar. The channels have an average diameter of 2.89 Å. Barium acetate exhibits channels towards which the methyl groups are oriented. The coordination number of Ba is nine (Figure 1a). Based on the metal-oxygen distance, the stability of the metal-linker (carboxylate) bond can be estimated.[51] This gives a first indication of the stability of the network, since often the metal linker bond is the weak point of the network.[43] In all three CPs the bond lengths between barium and the two oxygen atoms in the carboxylate groups are very similar; an average Ba–O distance is given in Figure 1. The strong electron attraction of trifluoroacetic acid increases the ionic character in the metal-oxygen bond as compared to acetic acid. Thus, the metal ion-linker bond is strengthened. If, on the other hand, fluorine is bound directly to the metal, the stabilizing effect is not as pronounced. In comparison with non-fluorinated CPs, the strong shortening effect of fluorine integration is particularly evident.

A low metal oxygen distance is unfortunately only an indication for the stability of the network. This assumption does not hold for the CPs investigated. However, the influence of various fluorine positions clearly manifests in different thermal behaviour (Figure 2). During the thermal decomposition of $BaF(CH_3COO)$, which has a direct metal ion - fluoride bond, BaF_2, $BaCO_3$ and acetone are formed at 504 °C, corresponding to a mass loss of 17% (Figure 2). The decomposition products were detected by X-ray powder diffraction measurements. The non-fluorinated barium coordination polymer $Ba(CH_3COO)_2$ decomposes at almost the same temperature (~500 °C) and barium carbonate and acetone are formed as well. The loss in mass corresponds to the release of acetone. Zhu et al. were able to show by comparing a triazolate framework with a direct metal-fluorine bond and a non-fluorinated triazolate framework that thermal stability can be increased by the structural motif of the direct metal-fluorine bond in coordination polymers.[52] In comparison, $Ba(CF_3COO)_2$ decomposes already at 366 °C, the lowest observed temperature here. This contradicts the statement of Chi Yang *et al.*[6,53] who found coordination polymers with perfluorinated linkers are more stable than the non-fluorinated compounds. Moreover, according to the HSAB theory,[44] fluorinated acids are therefore harder acids than non-fluorinated acids. Stable compounds are formed from equally hard and soft cations and anions. In our case, the barium ion is a soft cation, which forms more stable compounds with soft acids, here acetic acid. This results in a more stable metal ion-linker bond, which is expressed in the higher thermal stability of $Ba(CH_3COO)_2$ in comparison with $Ba(CF_3COO)_2$. In addition, the low decomposition temperature of $Ba(CF_3COO)_2$ can also be attributed to the high formation enthalpy of BaF_2,[49,54,55] which in this case is preformed to form a highly symmetric cubic barium fluoride lattice (see SI-II), thereby reducing the decomposition enthalpy.

$$Ba(CH_3COO)_2 \rightarrow Ba(CO_3)\ (s) + CH_3COCH_3\ (g) \quad (1)$$

$$Ba(CF_3COO)_2 \rightarrow BaF_2\ (s) + CF_3COF\ (g) + CO\ (g) + CO_2\ (g) \quad (2)$$

$$BaF(CH_3COO) \rightarrow 0.5\ Ba(CO_3)\ (s) + 0.5\ BaF_2\ (s) + 0.5\ CH_3COCH_3\ (g) \quad (3)$$

If the reaction products (see equations 1–3) of thermal decomposition are considered, it is noticeable that only 0.5 mole of gas is formed during the decomposition of barium acetate fluoride but one mole of gas is formed in the case of barium acetate instead of the 3 moles of gas formed in the case of barium trifluoroacetate. This shows that the decomposition of $Ba(CF_3COO)_2$ is entropically favoured and both the thermal stability and the stability against humidity limit its application range in MOFs and CPs. Several theoretical[56] and experimental[57] studies exist dealing with the water stability of and water storage in MOFs. The fluorine position in the network also has an influence on both the water vapour sorption as well as on the dissolution behaviour of the coordination polymers. Figure 4 shows the isotherms of water vapor sorption of the three coordination polymers and photos of the weighing pan during the measurement. A detailed explanation of what is shown on the pictures can be found in Section SI-III. The colourless powder (which is darker in the photo than the balance switch) can be seen in the pictures at the grain boundaries. The sorption isotherm of $Ba(CH_3COO)_2$ shows a significant increase in mass at a humidity of 90%. The images show that the powder has dissolved and that there is a solution on the weighing pan. The dissolution of the powder can be recognized by the fact that the grain boundaries are no longer visible (see red marked areas, Figure 4). When the air humidity

© 2021 The Authors. Zeitschrift für anorganische und allgemeine Chemie published by Wiley-VCH GmbH

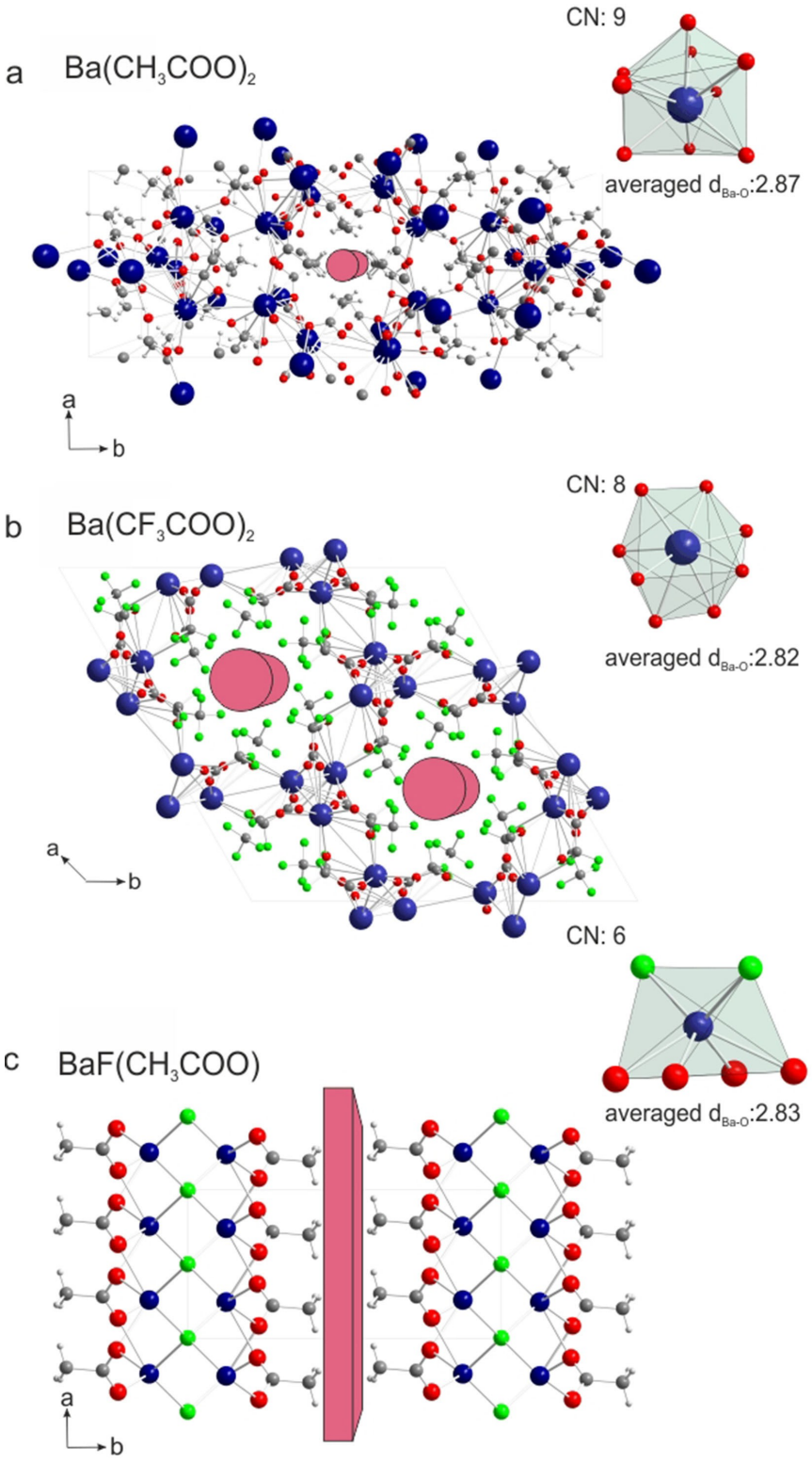

Figure 1. Crystal structures with the cavities (red) of the coordination polymers along the c-axis and local coordination environment of barium: a) $Ba(CH_3COO)_2$, b) $Ba(CF_3COO)_2$ with perfluorinated linker, c) $BaF(CH_3COO)$ with a direct metal-fluorine bond. Barium atom dark blue, fluorine atom green, oxygen atom red, carbon atom light grey, hydrogen atom white. Red rods indicate channels within the crystal structure.

© 2021 The Authors. Zeitschrift für anorganische und allgemeine Chemie published by Wiley-VCH GmbH

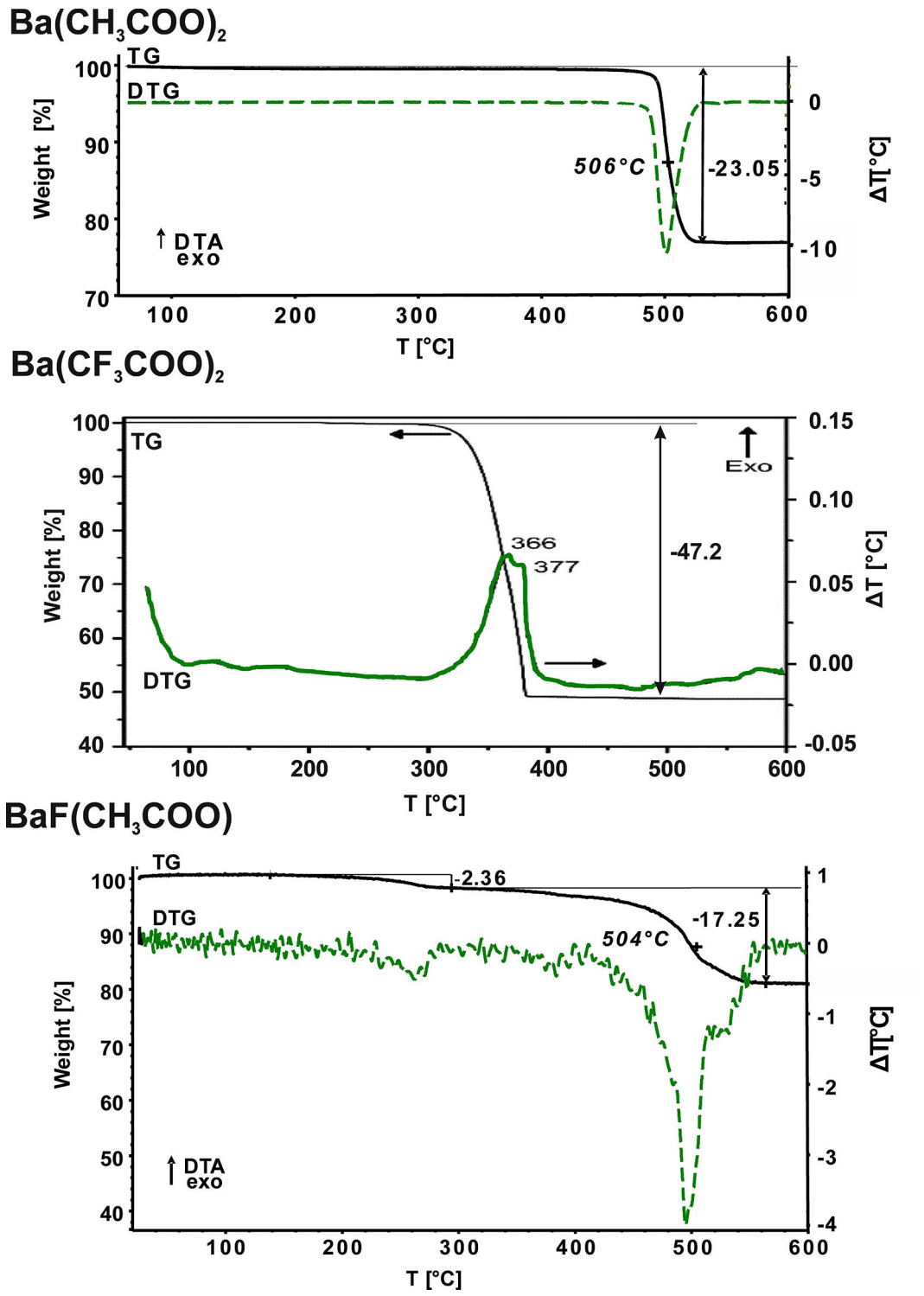

Figure 2. Comparison of thermoanalytical curves of barium acetate fluoride, barium acetate and bariumtrifluoracetate curves (green DTA curve, black TG curve) as well as the decomposition temperatures and the loss of mass. DTA curve and TG curve of $Ba(CF_3COO)_2$ are reprinted from K. Trauni Dissanayake *et al.*, Open-Framework Structure of Anhydrous $Sr(CF_3COO)$ and $Ba(CF_3COO)_2$, Inorg. Chem. 55 (2016) 170–176. With permission of the American Chemical Society. Copyright 2016 American Chemical Society.

is reduced, the barium acetate monohydrate crystallizes out of the solution. This can be seen from the 7% increase in mass at the end of the measurement. The difference in mass between barium acetate monohydrate and acetate anhydrate is 7%. Due to the large Ba^{2+} radius, Barium ions show higher coordination

 © 2021 The Authors. Zeitschrift für anorganische und allgemeine Chemie published by Wiley-VCH GmbH

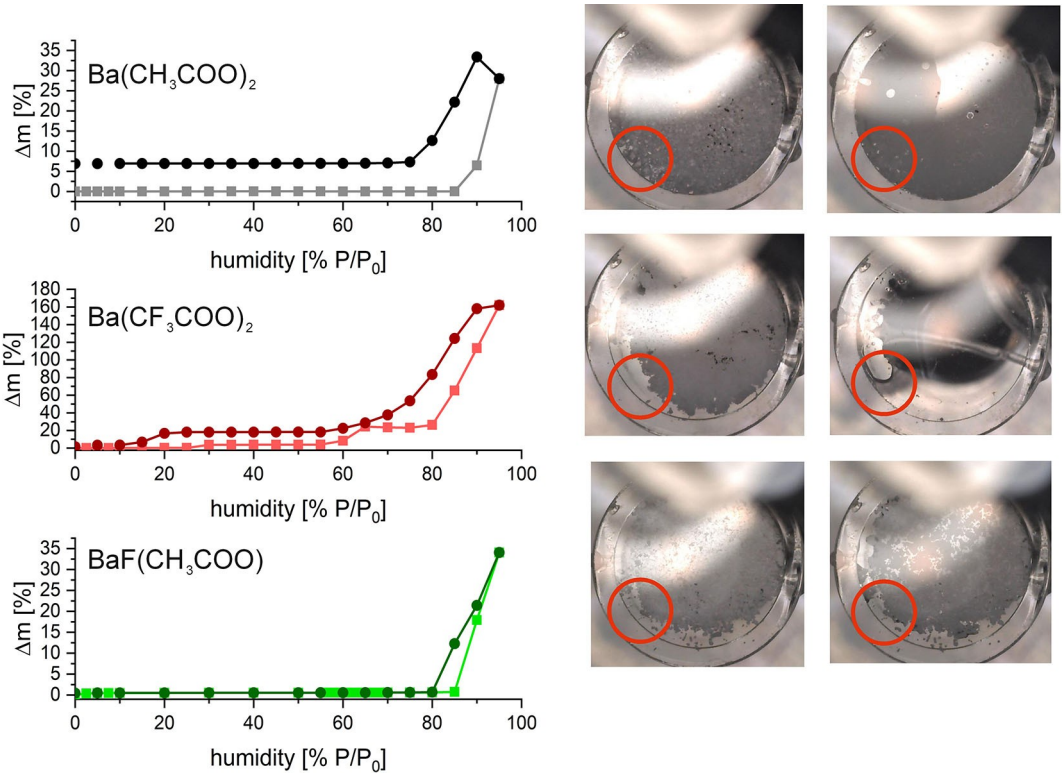

Figure 3. Comparison of isothermal curves for the dynamic vapour sorption (light colour)/desorption (dark colour) of water on $Ba(CH3COO)_2$ (black), $Ba(CF3COO)_2$ (red) and BaF(CH3COO) (green) and pictures of the weighing pan with the samples from the bird's eye view during the sorption measurement (left at 60 % humidity and right at 85 % humidity).

numbers and a higher tendency to form hydrates compared to other alkaline earth metal compounds.

This effect is intensified if the barium is still coordinated by electron withdrawing ligands, anions or linkers. This is the case with $Ba(CF_3COO)_2$. If the humidity is increased, it can be deduced from the distinct mass increase (cf. Figure 3) that the mono- and penta hydrates (3.5 % and 23 % increase) are formed. The photographs show that the substance dissolves (Figure 4). With the decrease of the air humidity a further plateau is recognized. On the basis of the difference in mass it cannot be decided whether the crystallising product is the $Ba(CF_3COO)_2 \cdot 4H_2O$ or a mixture of $Ba(CF_3COO)_2 \cdot H_2O$ and $Ba(CF_3COO)_2 \cdot 5H_2O$. All hydrates of $Ba(CF3COO)_2 \cdot nH_2O$ are known from the literature [36]. Despite the fluorinated hydrophobic channels, water penetrates the structure and forms various hydrates. The strong electronic pull of the perfluorinated linker reduces the electron density on the metal, which can be compensated by the free electron pairs of oxygen in water. Acetic acid and hydrofluoric acid are weak acids compared to trifluoroacetic acid and therefore the influence of these linkers on the electron density of the metal is less.

It is therefore surprising that the coordination network, which has a direct metal ion -fluoride bond and a lower coordination number of the barium atom, does not form a hydrate. In the sorption isotherm no plateau or increase is visible between 0 to 80 % humidity (Figure 3), which would indicate a hydration. The increase in mass above 85 % humidity is due to condensation of water on the weighing pan. No solution process can be seen on the photos (Figure 3). The demarcation between powder and weighing pan is maintained and the grain boundaries are visible on all pictures and remain

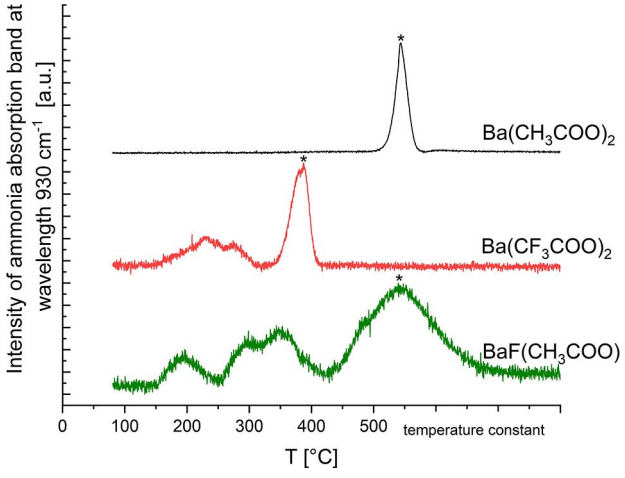

Figure 4. Temperature-programmed desorption of ammonia (NH_3-TPD) profiles of $Ba(CH_3COO)_2$, $Ba(CF_3COO)_2$, and $BaF(CH_3COO)$. The desorption temperature is plotted against the intensity of the absorption band of desorbed NH_3 at 930 cm^{-1}. (* thermal decomposition of the CPs).

© 2021 The Authors. Zeitschrift für anorganische und allgemeine Chemie published by Wiley-VCH GmbH

unchanged. If the water would accumulate between the layers or on the metal, an increase in mass would be observed at lower air humidity. This is astonishing in comparison to $Ba(CF_3COO)_2$, which forms different hydrates. Due to the low coordination number and the larger mean Ba–O distance, the barium in the $BaF(CH_3COO)$ has, in principle, a bit more space to store water. Also the layer spacing of 2.96 Å would allow the diffusion of water as well as the deposition of water (kinetic diameter of 2.65 Å[58,59]) between the layers.

The structural motif of a direct metal ion-fluoride bond prevents water absorption due to the hydrophobic character of the fluorine. This hydrophobic behaviour was also observed for AlF(*p*-BDC)[38] and Ga(OH,F)(*p*-BDC).[40] The structural M–F motif is suitable for preventing water accumulation at the metal center and thus prevents a step in the hydrolysis of MOFs and coordination polymers.

Temperature programmed desorption (TPD) of NH_3 was performed for probing the influence of the fluorine positions on the electron density on the metal. For this purpose, NH_3 is adsorbed on the sample, then loaded sample is heated. By heating the sample, NH_3 desorbs, which is detected by an IR spectrometer. The TPD of NH_3 is an important method for determining the number and strength of Lewis and Brønsted acid sites on the surface. Acidic centers on the surface include mainly not fully coordinated metal centers. A strong interaction between the metal centers and the free electron pair of NH_3 can be expected if the electron density on the metal is low. This strong interaction is shown by high desorption temperatures in the TPD curves. The TPD curves of the investigated CPs differ significantly from each other (Figure 4). Compared to $Ba(CF_3COO)_2$, $BaF(CH_3COO)$ releases ammonia at higher temperatures. This indicates the existence of stronger acidic centers in $BaF(CH_3COO)$. Based on the three maxima, it can be assumed that $BaF(CH_3COO)$, in contrast to $Ba(CF_3COO)_2$, has at least three various types of acidic centers, whereby only two various types of acidic centers can be distinguished. The strongly dominant signal in the TPD curves indicates the thermal decomposition of the samples. The signal is caused by the superposition of the absorption spectra of the decomposition products and cannot be assigned to ammonia. The decomposition temperatures of the substances agree well with the results of the thermal analysis. The BET surfaces of the examined CPs are quite small (see Table SI-IV). In the upper section it was assumed that the fluorinated linker reduces the electron density on the metal, whereby the metal (barium) interacts better with the electron pairs of the probe molecule (water). The probe molecule used in the TPD measurements is ammonia (NH_3), which also has a free electron pair, whereby it interacts with the metal of the CPs. The $BaF(CH_3COO)$ shows a stronger interaction with NH_3 – which can be seen from the high desorption temperature – and no interaction with water, which can be seen from the water vapor isotherm (Figure 3). Of all three CPs investigated, $Ba(CF_3COO)_2$ shows the best water adsorption and has the weakest acid centres. When attaching neutral molecules to the metals, the dipole moment and polarizability of the probe molecules should also be considered. Water has the higher dipole moment compared to NH_3, but has a lower polarizability.[60] Due to its high dipole moment, water interacts more strongly with hard cations, whereas the more polarizable NH_3 interacts better with soft cations. This is known from the fact hard alkali and alkaline earth metals in solution in the presence of NH_3 are more likely to form aqua complexes than ammine complexes, whereas the soft transition elements form ammine complexes.[61] The stronger the electronic pull of the linker in these Ba–CPs, the lower the electron density at the barium and the better water can be attached. If, on the other hand, barium in the CP is surrounded by linkers whose respective acids are weaker, NH_3 attaches more readily. Thus, the hardness of chemically equal metal centres can be controlled by the different fluorine positions.

However, for adsorption heat pumps that can be operated with water, water stability and absorption behaviour are important. These properties can be tuned by the various fluorine positions.

The layer structure or perfluorinated channels of the investigated compounds indicate potentially good ion conducting properties. Therefore, we investigated how the compounds behave as anode material in lithium ion batteries (LIB). We tested how the fluorine position affects the cycle stability, the capacity, and the electronic behaviour.

The CPs were used as electrode materials for lithium ion batteries with lithium metal foils as counter electrodes. To build the anode a paste was produced from the electroactive material with carbon black conducting additive and PVDF binder in N-methyl-2-pyrrolidine (NMP) which was applied on to a copper foil.

Scheme 1 shows the possible electrochemical anode reaction where the Li-ion insertion takes place on oxygen atoms of the carboxylate. For charge neutralization of the active material, the barium cations must therefore be reduced. The cyclic voltammetry test has been implemented at the same scan rate of 0.1 $mV\,s^{-1}$ and is performed for $Ba(CH_3COO)_2$, $Ba(CF_3COO)_2$ and $BaF(CH_3COO)$ (Figure 5). Reproducible, closed curves were measured with all three different anode materials. The different

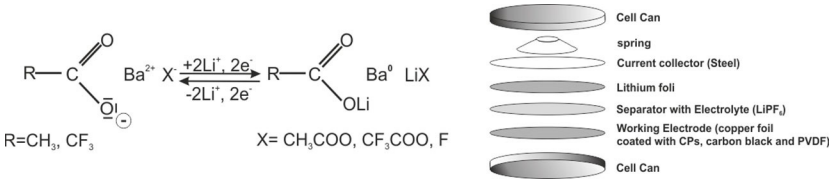

Scheme 1. Lithium storage mechanism of CP at molecular structure level and schematic structure of the LIBs.

© 2021 The Authors. Zeitschrift für anorganische und allgemeine Chemie published by Wiley-VCH GmbH

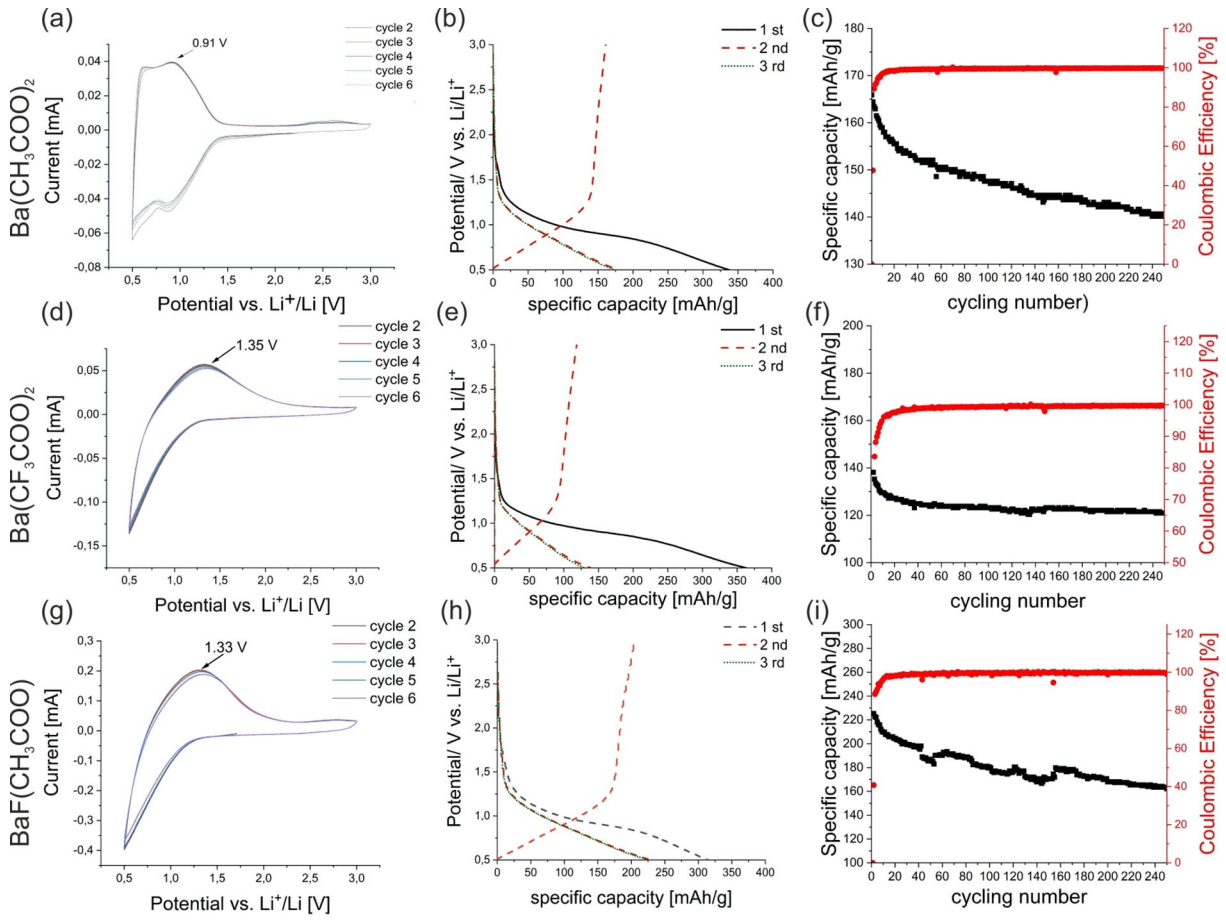

Figure 5. Electrochemical properties of $Ba(CH_3COO)_2$, $Ba(CF_3COO)_2$ and $BaF(CH_3COO)$. (a,d,g) cyclic voltammograms at a scan rate of 0.10 mV s^{-1}. (b, e, h) Typical discharge/charge curves at a current density of 0.1 A g^{-1}. (c, f, i) Cycling performance at 0.1 A g^{-1}.

shapes of the cathodic peaks and the very broad anodic peaks indicate asymmetric redox processes in all investigated materials.[62] This effect is particularly pronounced when fluorine is integrated into the CP. In the case of $BaF(CH_3COO)_2$ and $Ba(CF_3COO)_2$, the very broad anodic peaks are hardly visible. Another reason for the barely recognizable cathodic peak could be that the Li^+ does not disinsert after deposition at the anode. If the voltages of the reduction peaks of the different materials are compared, it is noticeable that the voltage can be significantly increased by incorporating fluorine into the CPs and that $Ba(CF_3COO)_2$ has the highest voltage. The increase in voltage can always be observed as the metal ion-linker bond strengthens.[51] The position of the strongly electron-withdrawing fluorine in the network has a pronounced influence on the electron density at the barium and thus on the stability of the barium-linker bond. For the binding of Li^+ ions to carbonyl oxygen, the free electron pair of the oxygen must leave the p-orbital, which is more difficult given the strong interaction with barium, which is apparent in the short bonding distance between barium and oxygen.[51,62]

The impact of the Ba–O bond in these CPs is also evident when comparing the voltages of the reduction peaks with the M–O distance of the three anode materials. With decreasing mean M–O distance the voltage increases. The stronger the carboxylate-barium interaction, the higher voltage must be to break this interaction and deposit lithium ion on the carboxylate. Figure 5 displays the charge/discharge curves of the three CPs electrodes. All electrodes show a significantly higher capacity in the first cycle than the theoretically calculated capacity (see Table 1). The irreversible capacity should be ascribed to the formation of solid electrolyte interface (SEI) which is consistent with discharge/charge curves results.[63–65] The $BaF(CH_3COO)$ electrode shows the highest capacity of 219 mAh g^{-1} at 0.1 A g^{-1} among the three investigated materials. The investigated CPs show a low theoretical capacity; therefore, they are not suitable as anode materials for Li batteries (see Table 1). On the other hand, the cycling performance of CPs was also tested on 250 cycles (Figure 5). The capacity decreases for all Cps with increasing number of cycles, because of an activation process and dissolution of active materials in electrolytes. The initial coulombic efficiency is low which could be ascribed to irreversible decomposition of the electrolyte and a limited reversibility of lithiation/ delithiation process -this is common for organic electrodes.[66,67] The channels of $Ba(CF_3COO)_2$ in which the Li^+ could be deposited are stabilized by the electrostatic interaction of the fluorine,

© 2021 The Authors. Zeitschrift für anorganische und allgemeine Chemie published by Wiley-VCH GmbH

Table 1. Overview of the capacities, voltage of reduction peak and the fading rate of three CPs.

Electrode material	Molecular weight [g/mol]	Theoretical capacity [mAh/g]	Voltage of reduction peak [V]	Capacity of the 1st cycle [mAh/g]	Capacity of the 2nd cycle [mAh/g]	Fading rate [%]
$Ba(CH_3COO)_2$	255.4	209.88	0.95	335.6	172.9	0.38
$Ba(CF_3COO)_2$	363.3	147.54	1.35	362.5	134.9	0.27
BaF (CH_3COO)	215.3	248.97	1.33	374.4	219.3	0.45

which could be connected to the fact that this material shows the lowest fading rate of the examined CPs. In addition, the negatively lined channels allow a better incorporation of the Li^+ cations. $Ba(CH_3COO)_2$ also has a channel system which, unlike $Ba(CF_3COO)_2$, is not lined with fluorine so the fading rate is therefore higher than that of $Ba(CF_3COO)_2$.

The $Ba(CF_3COO)_2$ has the lowest fading rate among the examined CPs. The $Ba(CF_3COO)_2$ has perfluorinated channels in which the Li^+ can be easily deposited. The electrostatic interaction between fluorine and lithium stabilizes the structure. $Ba(CH_3COO)_2$ also has a channel system which, in contrast to $Ba(CF_3COO)_2$, is not lined with fluorine, so that the fading rate is higher than that of $Ba(CF_3COO)_2$. $BaF(CH_3COO)$ with its direct barium-fluorine bond has the highest fading rate. In this case fluorine does not stabilize the deposition of Li^+ in the channels. The layers are only held together by the van der Waals interactions of the acetate groups. The Li^+ could settle in the gap between the layers. This leads to a distortion of the structure, which can lead to the collapse of the crystal structure of the host lattice.[68–70]

The various fluorine positions favour or worsen properties that are important for the development of anode materials. The $Ba(CF_3COO)_2$ shows a better cycling performance, but the BaF (CH_3COO) is thermally much more stable. Compared to conventional organic electrodes,[71] the electroactive $BaF(CH_3COO)$ shows a relatively high decomposition temperature and thus the structural motif of a direct metal ion – fluoride bond offers the possibility to build safe batteries. The water-repellent property is particularly useful for being used as an anode material for LIB. This prevents the side reaction of the electrolyte ($LiPF_6$) with water, which leads to HF, which damages the anode.[24]

Conclusions

Fluorinated CPs are innovative materials for the energy transition, especially absorption heat pumps and lithium-ion batteries (LIB). The fluorine position in the network crucially influences the material properties. The CPs reported in this work contain the same carbon skeleton of the linker, the same metal cation and a similar chemical composition: barium acetate fluoride $BaF(CH_3COO)$ as a coordination polymer with a direct metal-fluorine bond, barium trifluoroacetate $Ba(CF_3COO)_2$ as a coordination polymer with a perfluorinated linker, and non-fluorinated barium acetate $Ba(CH_3COO)_2$. As anode material in LIBs, the fluorine position in the network has a strong influence on the cycle stability as well as the electronic behaviour. If fluorine is integrated into the network via the perfluorinated linker, as in the case of $Ba(CF_3COO)_2$, a better cycle stability is observed than in $BaF(CH_3COO)$. This can be attributed to a better uptake of Li^+ in the fluorinated channels. When fluorine is bound directly to the metal, thermal stability is increased compared to CPs, which consist of the metal cation and perfluorinated linkers. The high thermal stability is attributed to the low decomposition enthalpy of $BaF(CH_3COO)$. The thermal stability of the individual components is important for the safety of possible batteries. The structural motif of a direct metal-fluorine bond is suitable for preventing water accumulation near the metal center, thus preventing a step in the hydrolysis of MOFs and coordination polymers. This finding is based on dynamic vapour sorption measurements of BaF (CH_3COO). The low coordination number of the metal (steric interaction) and the directly coordinated fluorine (electronic interaction) would in principle favour hydrate formation. However, the hydrophobic effect of the fluorine prevents hydrate formation and water accumulation on the metal. Not only the hydrophobicity of CPs can be controlled by the different fluorine positions, but also the strength of the acid centers in the network. Temperature programmed desorption measurements (TPD) with NH_3 show that the strength of the acid centres is increased by the direct coordination of the strongly polarizing fluorine on the metal. In contrast, significantly weaker acid centres are observed with $Ba(CF_3COO)_2$. Due to the different absorption behaviour of the probe molecules (H_2O and NH_3), conclusions can be drawn about the hard and soft barium centres. The position of the fluorine in the CP has a significant influence on the electron density on the metal and thus the hardness of the metal centres can be controlled.

The structural motif of a direct metal ion - fluoride bond is interesting as a new design idea for CPs in LIBs, absorption systems, and catalysis due to its thermal behaviour and hydrophobic properties.

Acknowledgements

We thank Dr. T. Krahl (HU Berlin) for DTA-TG measurements, Mrs Annett Zimathies (BAM) and Carsten Prinz (BAM) for BET and water sorption measurements, Sigrid Bäßler (HU Berlin) for TPD

 © 2021 The Authors. Zeitschrift für anorganische und allgemeine Chemie published by Wiley-VCH GmbH

measurements. Open access funding enabled and organized by Projekt DEAL.

Keywords: alkaline earth metal coordination polymers · water stability · fluorine coordination · lithium-ion battery

[1] M. Eddaoudi, J. Kim, N. Rosi, D. Vodak, J. Wachter, M. O'Keeffe, O. M. Yaghi, *Science* **2002**, *295* (5554), 469–472.
[2] B. Salvi, K. Subramanian, *Renewable Sustainable Energy Rev.* **2015**, *51*, 1132–1155.
[3] L. E. Kreno, K. Leong, O. K. Farha, M. Allendorf, R. P. Van Duyne, J. T. Hupp, *Chem. Rev.* **2012**, *112* (2), 1105–1125.
[4] A. Rezk, R. Al-Dadah, S. Mahmoud, A. Elsayed, *Proc. Inst. Mech. Eng., Part C* **2013**, *227* (5), 992–1005.
[5] D. Saha, R. Sen, T. Maity, S. Koner, *Dalton Trans.* **2012**, *41* (24), 7399–7408.
[6] C. Yang, X. Wang, M. A. Omary, *J. Am. Chem. Soc.* **2007**, *129* (50), 15454–15455.
[7] C. Janiak, S. K. Henninger, *Nachr. Chem.* **2013**, *61* (5), 520–523.
[8] F. Jeremias, A. Khutia, S. K. Henninger, C. Janiak, *J. Mater. Chem.* **2012**, *22* (20), 10148–10151.
[9] P. Küsgens, M. Rose, I. Senkovska, H. Fröde, A. Henschel, S. Siegle, S. Kaskel, *Microporous Mesoporous Mater.* **2009**, *120* (3), 325–330.
[10] G. Férey, *Chem. Soc. Rev.* **2008**, *37* (1), 191–214.
[11] J. W. Choi, D. Aurbach, *Nat. Rev. Mater.* **2016**, *1* (4), 1–16.
[12] C. Li, X. Lou, M. Shen, X. Hu, Z. Guo, Y. Wang, B. Hu, Q. Chen, *ACS Appl. Mater. Interfaces* **2016**, *8* (24), 15352–15360.
[13] N. L. Rosi, J. Eckert, M. Eddaoudi, D. T. Vodak, J. Kim, M. O'Keeffe, O. M. Yaghi, *Science* **2003**, *300* (5622), 1127–1129.
[14] S. T. Meek, J. J. Perry IV, S. L. Teich-McGoldrick, J. A. Greathouse, M. D. Allendorf, *Cryst. Growth Des.* **2011**, *11* (10), 4309–4312.
[15] P. Pachfule, Y. Chen, J. Jiang, R. Banerjee, *Chem. Eur. J.* **2012**, *18* (2), 688–694.
[16] C. Serre, *Angew. Chem.* **2012**, *124* (25), 6152–6154.
[17] K. Peikert, F. Hoffmann, M. Fröba, *CrystEngComm* **2015**, *17* (2), 353–360.
[18] S. He, X. Zhou, Z. Li, J. Wang, L. Ma, S. Yang, *ACS Appl. Mater. Interfaces* **2017**, *9* (32), 26907–26914.
[19] G. G. Amatucci, N. Pereira, *J. Fluorine Chem.* **2007**, *128* (4), 243–262.
[20] S. Yonezawa, M. Yamasaki, M. Takashima, *J. Fluorine Chem.* **2004**, *125* (11), 1657–1661.
[21] M. Vandichel, J. Hajek, F. Vermoortele, M. Waroquier, D. E. De Vos, V. Van Speybroeck, *CrystEngComm* **2015**, *17* (2), 395–406.
[22] L. Zhan, S. Yang, Y. Wang, Y. Wang, L. Ling, X. Feng, *Adv. Mater. Interfaces* **2014**, *1* (4), 1300149.
[23] J. L. Adcock, P. F. Fulvio, S. Dai, *J. Mater. Chem. A* **2013**, *1* (33), 9327–9331.
[24] T. Nakajima, H. Groult, *Fluorinated materials for energy conversion*, Elsevier **2005**.
[25] I. Abdi, J. Lhoste, M. Leblanc, V. Maisonneuve, J.-M. Grenèche, G. Viau, A. B. Ali, *J. Fluorine Chem.* **2015**, *173*, 23–28.
[26] K. Adil, A. Le Bail, M. Leblanc, V. Maisonneuve, *Inorg. Chem.* **2010**, *49* (5), 2392–2397.
[27] A. Cadiau, C. Martineau, M. Leblanc, V. Maisonneuve, A. Hémon-Ribaud, F. Taulelle, K. Adil, *J. Mater. Chem.* **2011**, *21* (11), 3949–3951.
[28] J. Lhoste, M. Body, C. Legein, A. Ribaud, M. Leblanc, V. Maisonneuve, *J. Solid State Chem.* **2014**, *217*, 72–79.
[29] V. Pimenta, Q. H. H. Le, L. Clark, J. Lhoste, A. Hémon-Ribaud, M. Leblanc, J.-M. Grenèche, G. Dujardin, P. Lightfoot, V. Maisonneuve, *Dalton Trans.* **2015**, *44* (17), 7951–7959.
[30] V. Pimenta, Q. H. H. Le, A. Hemon-Ribaud, M. Leblanc, V. Maisonneuve, J. Lhoste, *J. Fluorine Chem.* **2016**, *188*, 164–170.
[31] V. Pimenta, J. Lhoste, A. Hémon-Ribaud, M. Leblanc, J.-M. Grenèche, L. Jouffret, A. Martel, G. Dujardin, V. Maisonneuve, *Cryst. Growth Des.* **2015**, *15* (9), 4248–4255.
[32] M. Smida, J. Lhoste, V. Pimenta, A. Hémon-Ribaud, L. Jouffret, M. Leblanc, M. Dammak, J.-M. Grenèche, V. Maisonneuve, *Dalton Trans.* **2013**, *42* (44), 15748–15755.
[33] A. M. Goforth, C.-Y. Su, R. Hipp, R. B. Macquart, M. D. Smith, H.-C. zur Loye, *J. Solid State Chem.* **2005**, *178* (8), 2511–2518.
[34] T. Hagino, S. Hiryu, S. Fujioka, H. Riquimaroux, Y. Watanabe, *Adaptive SONAR sounds by echolocating bats*, 5th International Symposium on Underwater Technology, Tokyo, Japan, APR 17–20; IEEE: Tokyo, Japan **2007**, pp 647–651.
[35] I. M. Pepperberg, *The Oxford Handbook of Comparative Evolutionary Psychology*, J. Vonk, T. K. Shackelford, Eds. Oxford University Press: New York **2012**, pp 297–319.
[36] C.-Y. Su, A. M. Goforth, M. D. Smith, P. Pellechia, H.-C. zur Loye, *J. Am. Chem. Soc.* **2004**, *126* (11), 3576–3586.
[37] K. Barthelet, K. Adil, F. Millange, C. Serre, D. Riou, G. Férey, *J. Mater. Chem.* **2003**, *13* (9), 2208–2212.
[38] L. Liu, X. Wang, A. J. Jacobson, *Dalton Trans.* **2010**, *39* (7), 1722–1725.
[39] G. Férey, M. Latroche, C. Serre, F. Millange, T. Loiseau, A. Percheron-Guégan, *Chem. Commun.* **2003**, (24), 2976–2977.
[40] A. Boutin, D. Bousquet, A. I. U. Ortiz, F. o.-X. Coudert, A. H. Fuchs, A. Ballandras, G. Weber, I. Bezverkhyy, J.-P. Bellat, G. Ortiz, *J. Phys. Chem. C* **2013**, *117* (16), 8180–8188.
[41] M. De Toni, R. Jonchiere, P. Pullumbi, F. X. Coudert, A. H. Fuchs, *ChemPhysChem* **2012**, *13* (15), 3497–3503.
[42] J. B. DeCoste, G. W. Peterson, B. J. Schindler, K. L. Killops, M. A. Browe, J. J. Mahle, *J. Mater. Chem. A* **2013**, *1* (38), 11922–11932.
[43] J. J. Low, A. I. Benin, P. Jakubczak, J. F. Abrahamian, S. A. Faheem, R. R. Willis, *J. Am. Chem. Soc.* **2009**, *131* (43), 15834–15842.
[44] R. G. Pearson, *J. Am. Chem. Soc.* **1963**, *85* (22), 3533–3539.
[45] I. Akhmetova, S. Beyer, K. Schutjajew, T. Tichter, M. Wilke, C. Prinz, I. C. Martins, D. Al-Sabbagh, C. Roth, F. Emmerling, *CrystEngComm* **2019**, *21* (39), 5958–5964.
[46] A.-A. Al-Terkawi, G. Scholz, A. G. Buzanich, S. Reinsch, F. Emmerling, E. Kemnitz, *Dalton Trans.* **2017**, *46* (18), 6003–6012.
[47] A.-A. Al-Terkawi, G. Scholz, C. Prinz, F. Emmerling, E. Kemnitz, *Dalton Trans.* **2019**, *48* (19), 6513–6521.
[48] S. Zänker, G. Scholz, M. Heise, F. Emmerling, E. Kemnitz, *CrystEngComm* **2020**.
[49] J. Farjas, J. Camps, P. Roura, S. Ricart, T. Puig, X. Obradors, *Thermochim. Acta* **2012**, *544*, 77–83.
[50] K. T. Dissanayake, L. M. Mendoza, P. D. Martin, L. Suescun, F. A. Rabuffetti, *Inorg. Chem.* **2015**, *55* (1), 170–176.
[51] L. Wang, C. Mou, B. Wu, J. Xue, J. Li, *Electrochim. Acta* **2016**, *196*, 118–124.
[52] A.-X. Zhu, J.-B. Lin, J.-P. Zhang, X.-M. Chen, *Inorg. Chem.* **2009**, *48* (8), 3882–3889.
[53] C. Yang, X. Wang, M. A. Omary, *Angew. Chem. Int. Ed.* **2009**, *48* (14), 2500–2505.
[54] T. Araki, I. Hirabayashi, *Supercond. Sci. Technol.* **2003**, *16* (11), R71.
[55] T. Y. Glazunova, A. Boltalin, P. Fedorov, *Russ. J. Inorg. Chem.* **2006**, *51* (7), 983–987.
[56] J. A. Greathouse, M. D. Allendorf, *Journal of the American Chemical Society* **2006**, *128* (33), 10678–10679.
[57] A. M. Fracaroli, H. Furukawa, M. Suzuki, M. Dodd, S. Okajima, F. Gándara, J. A. Reimer, O. M. Yaghi, *J. Am. Chem. Soc.* **2014**, *136* (25), 8863–8866.
[58] A. L. McClellan, H. Harnsberger, *J. Colloid Interface Sci.* **1967**, *23* (4), 577–599.

 © 2021 The Authors. Zeitschrift für anorganische und allgemeine Chemie published by Wiley-VCH GmbH

[59] P. L. Silvestrelli, M. Parrinello, *Phys. Rev. Lett.* **1999**, *82* (16), 3308.
[60] D. Yarkony, *Modern electronic structure theory*, World Scientific **1995**; Vol. 2.
[61] K. A. Hofmann, *Anorganische Chemie*, Springer-Verlag **2013**.
[62] L. Wang, C. Mou, Y. Sun, W. Liu, Q. Deng, J. Li, *Electrochim. Acta* **2015**, *173*, 235–241.
[63] L. Wang, Z. Schnepp, M. M. Titirici, *J. Mater. Chem. A* **2013**, *1* (17), 5269–5273.
[64] L. Wang, H. Li, M. Courty, X. Huang, E. Baudrin, *J. Power Sources* **2013**, *232*, 165–172.
[65] L. Zhao, J. Zhao, Y. S. Hu, H. Li, Z. Zhou, M. Armand, L. Chen, *Adv. Energy Mater.* **2012**, *2* (8), 962–965.
[66] J. Wu, X. Rui, G. Long, W. Chen, Q. Yan, Q. Zhang, *Angew. Chem. Int. Ed.* **2015**, *54* (25), 7354–7358.
[67] J. Wu, X. Rui, C. Wang, W. B. Pei, R. Lau, Q. Yan, Q. Zhang, *Adv. Energy Mater.* **2015**, *5* (9), 1402189.
[68] D. Aurbach, A. Zaban, Y. Ein-Eli, I. Weissman, O. Chusid, B. Markovsky, M. Levi, E. Levi, A. Schechter, E. Granot, *J. Power Sources* **1997**, *68* (1), 91–98.
[69] W. Luo, X. Chen, Y. Xia, M. Chen, L. Wang, Q. Wang, W. Li, J. Yang, *Adv. Energy Mater.* **2017**, *7* (24), 1701083.
[70] S. Goriparti, E. Miele, F. De Angelis, E. Di Fabrizio, R. P. Zaccaria, C. Capiglia, *J. Power Sources* **2014**, *257*, 421–443.
[71] S. Gottis, A.-L. Barrès, F. Dolhem, P. Poizot, *ACS Appl. Mater. Interfaces* **2014**, *6* (14), 10870–10876.

Manuscript received: October 2, 2020
Revised manuscript received: November 21, 2020

 © 2021 The Authors. Zeitschrift für anorganische und allgemeine Chemie published by Wiley-VCH GmbH